Article

Kaolin Clay-Based Geopolymer for Ionic Thermoelectric Energy Harvesting

Guido Goracci,* Mary B. Ogundiran,* Mohamad Barzegar, Amaia Iturrospe, Arantxa Arbe, and Jorge S. Dolado

Read Online

ACCESS | Metrics & More | Article Recommendations

ABSTRACT: Geopolymers, a class of sustainable inorganic materials derived from natural and recycled resources, hold promise for various applications, including thermoelectric power generation. This study delves into the thermoelectric properties of Ikere white (IKW)-geopolymer, derived from kaolin clay, by employing rigorous measurements of thermal conductivity, electrical conductivity, and Seebeck coefficient. The investigation elucidates the pivotal role of temperature and ions in shaping the thermoelectric performance of IKW-geopolymer. Electrical conductivity analysis pinpoints ions within the geopolymer's channels as primary contributors. Beyond a critical temperature, the evaporation of bulk water triggers a transition of charge carriers from one- to three-dimensional motion, resulting in reduced conductivity. The Seebeck coefficient exhibits a range from −182 to 42 μV/K, with its time-dependent profile suggesting that ions potentially drive thermoelectricity in cementitious materials. Notably, a unique transition from n-type to p-type behavior was observed in the geopolymer, opening new avenues for ionic thermoelectric capacitors. These insights advance our understanding of thermoelectric behavior in geopolymers and have the potential to propel the development of novel building materials for energy conversion applications.
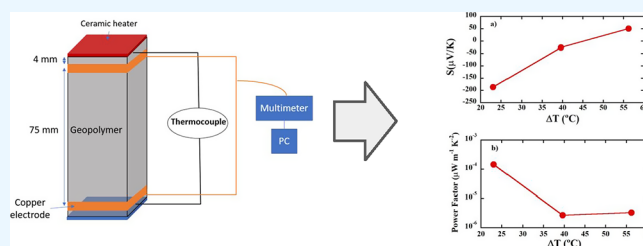
INTRODUCTION

The ongoing reliance on nonrenewable energy sources presents a significant challenge for the global community. This dependence not only perpetuates environmental degradation through the emission of harmful pollutants and greenhouse gases but also threatens our finite resources. To address this pressing issue, there is a growing need to explore new, innovative solutions that promote energy efficiency and reduce our reliance on nonrenewable energy sources. One solution that has the potential to make a significant impact is the use of thermoelectric materials.

This technology is based on the Seebeck effect, a phenomenon where a temperature difference between two ends of a material generates an electrical voltage, allowing capturing and converting the waste heat into usable electricity. The overall performance of a thermoelectric material is measured by the figure of merit, $ZT = S^2\sigma T/\kappa$, which is determined by the operating temperature T and three intrinsic thermoelectric properties such as the Seebeck coefficient (S), electrical conductivity (σ), and thermal conductivity (κ).

Developing thermoelectric materials would play a vital role in reducing carbon emissions and improving energy efficiency in various applications. The recovery of waste heat from industrial processes is a particularly promising area for thermoelectric materials.[1,2] High-temperature waste heat,

typically generated at temperatures above 600 °C, can come from sources such as furnace exhausts, boilers, and chemical reactions.[3] Additionally, low-grade waste heat, typically at temperatures below 150 °C, can be recovered from sources such as data centers.[4] By capturing and converting this waste heat into usable electricity, thermoelectric materials will contribute to significant energy savings and reductions in greenhouse gas emissions in various industrial sectors. Thermoelectrics can also be integrated into building structures, such as walls, floors, and roofs, providing a sustainable and efficient solution for waste heat recovery and energy harvesting. The integration of thermoelectric materials into smart cities infrastructure can make them more energy-efficient and self-sustaining.
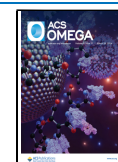
Thermoelectric materials have been rapidly advancing in recent years, leading to the development of a wide range of materials with unique properties and potential applications.[5−7] Some of the most promising materials include bismuth

telluride,[8,9] skutterudites,[10,11] and silicon−germanium,[12] which have high figure of merit (ZT) values and high thermoelectric performance. However, one major obstacle to the widespread adoption of thermoelectrics is the cost of these materials. To overcome this challenge, an innovative approach is to focus on materials that are cheaper and more widely available, even if they have lower ZT values like thermoelectric cementitious materials. These materials can be easily scaled up and integrated into building structures, providing a sustainable and efficient solution for waste heat recovery and energy harvesting in smart cities.

The development of cement-based materials with enhanced thermoelectric properties has been an active area of research in recent years. One of the widely adopted strategies is the incorporation of functional fillers into the cement matrix, which imparts electronic thermoelectric effects to the composite. Researchers have experimented with various types and contents of functional fillers, such as nanostructured graphene and zinc oxide, with the aim of improving the thermoelectric properties.[13−24] Recently, there has been a growing interest in studying the thermoelectric behavior of geopolymers. This is because they exhibit a higher Seebeck coefficient than normal cement paste and hold potential as a functional building material.[25−28]

In this framework, the potentials of geopolymers made from Nigerian kaolin clays (Ikere white (IKW)) as cheap, sustainable and eco-friendly alternative to traditional thermoelectric materials were investigated in this study.

The term "geopolymer" was first introduced by Joseph Davidovits for a new class of inorganic materials that are produced from the reaction of metakaolin in an alkaline environment at low temperatures.[29] Geopolymers are amorphous aluminosilicate materials with a tridimensional structure. They are produced from chemical reactions involving alkali hydroxide/silicate solutions with reactive alumina and silica in precursors such as metakaolin, calcined local kaolin clay, fly ash, and waste aluminosilicate materials. During geopolymerization reactions, each dissolved Al^{3+} replaces Si^{4+} in 4-fold coordination with respect to oxygen, leading to the creation of a negative charge. The presence of cations (e.g., Na^+, K^+) either maintains the charge balance (free cations) in the geopolymer matrix or is actively bound (structural cations) to the matrix.[30] Generally, the empirical formula of geopolymer is represented by $Mn[-(SiO_2)z\text{-}AlO_2]n\cdot wH_2O$, where M is alkali metals, particularly K, Na; n is the degree of polycondensation; z = 1, 2, 3 or ≫3; and w is the number of water molecules in its pore.[29]

Unlike traditional cement, which is made by heating limestone and clay, geopolymers are made from geological materials, including metakaolin, calcined kaolinite clay, and industrial byproducts and waste materials such as fly ash and slag.[31−35] This makes them a more sustainable and eco-friendly alternative to traditional cementitious materials.[36−38]

The investigation of the thermoelectric properties of IKW-geopolymer was conducted using a comprehensive methodology. Initial steps involved the characterization of the structural properties of the raw clay and calcined clay to determine its suitability as a geopolymer precursor, utilizing infrared spectroscopy, X-ray diffraction, and thermogravimetric analysis. The geopolymerization process was examined through isothermal conduction calorimetry. The thermoelectric behavior of the resulting geopolymer was evaluated through the measurement of physical properties that determine the figure

of merit (thermal conductivity, Seebeck coefficient, and electrical conductivity). Given that significant variations in electrical conductivity and Seebeck coefficient can occur, the focus was placed on comprehending such physical properties to better understand the mechanisms influencing the performance of the geopolymer as a thermoelectric. In particular, impedance spectroscopy and Seebeck coefficient measurements were performed to study the temperature-dependent movements of mobile charges and the response of the IKW-geopolymer to temperature gradients. Notably, the sample was characterized by a significant inherent voltage ($V = -106$ mV), necessitating the implementation of a unique experimental design to minimize its contribution and focus solely on the thermoelectric effect.

■ MATERIALS AND METHODS

Materials. The kaolin containing clay tagged IKW was obtained from a deposit in Ekiti State, Nigeria. Samples of both raw and calcined clay are shown in Figure 1.
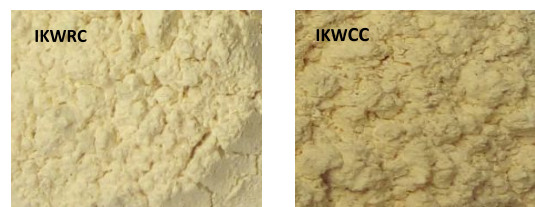

Figure 1. Pictures of raw (IKWRC) and calcined (IKWCC) IKW clay.

NaOH pellets (Mol wt: 40 g/mol, Sigma-Aldrich Germany) and sodium silicate solution (Density 1.39 g/mL; 12.0 to 13.0% Si based; 13.4 to 14.0% NaOH basis) purchased from Sigma-Aldrich USA were used to prepare alkaline silicate solution. 8 M $NaOH/Na_2SiO_3$ (1:1) solution was used as the activator prepared by dissolving the appropriate mass of NaOH pellets in deionized water and allowed to cool to room temperature before mixing with silicate activator and left for 24 h before use. Calcined IKW (IKWCC) was mixed with 8 M $NaOH/Na_2SiO_3$ solution to produce geopolymer (IKWG). The activator concentration was chosen based on previous studies on Nigerian clay geopolymers.[39] The ratio of the activator to the IKWCC was 0.63. The clay and the activator were mixed with a Hobart electric mixer (Heidolph. Hei-Torque 400 with a speed range of 200−2000 rpm) for 90 s, waited for 60 s, and then mixed for 90 s at 1200 rpm. The geopolymer paste was cast into prismatic molds. The cast pastes in the molds were compacted by vibration on an end-to-end shaker (Ovan) at 125 rpm for about 5 min and thereafter sealed with a vinyl sheet to prevent moisture evaporation. The sample was demolded after 2 days, stored in sealed plastic materials, and cured at room temperature for 28 days before characterization.

Chemical and Structural Characterization. Thermogravimetric analysis/derivative thermogravimetric (TGA/DTG) was performed on the raw IKW clay with a TA Instrument TGA Q500 to determine the thermal reactions and dehydroxylation (calcining) temperature of the clay. About 100 mg of the sample was placed in a platinum crucible. The measurement was carried out at a temperature between 30 and 900 °C at a heating rate of 10 °C min^{-1} in a Nitrogen atmosphere (100 mL min^{-1}). The raw clay was therefore

subjected to thermal treatment at its dehydroxylation temperature as revealed from TGA/DTG results in an electric programmable furnace (Nabertherm GmbH, Germany). The oxide composition of the calcined clay was determined using a sequential X-ray fluorescence (XRF) spectrometer (PANalytical AXIOS). To determine the mineralogical phases, the amorphous and crystalline nature of the raw and calcined clays were identified with Bruker X-ray diffractometer (D8 Advance, US). The sample was analyzed using 2θ range from 10 to 90° with a scan rate of 0.05°. The average measuring time was 50 s/point. The CuKα radiation (λ = 1.5418 Å) was generated at 40 kV and 40 mA. The XRD patterns were analyzed using Diffrac.EVA v.2.1 software. Attenuated total reflectance-Fourier transform infrared (ATR-FTIR) spectroscopy was used to determine the main characteristic chemical functional groups in the raw and calcined clay. The spectrometer was equipped with a diamond crystal plate. A few milligrams of the samples were placed on the plate. Absorption spectra were measured on an ATR-FTIR spectrometer (FTIR-6300/ATR-6000) set to scan wavelength across a range of 4000 to 500 cm^{-1} with a resolution of 4 cm^{-1} and 200 scans. Isothermal conduction calorimetry was done using a 16 channel isothermal conduction calorimeter (TAM AIR, Thermometric AB, Sweden) to ascertain the geopolymer formation from the alkali/silicate reaction of IKW calcined clay. The temperature of the calorimeter was set at 25 °C, to match the temperature used for the curing of geopolymer. Water (5 g) was used as a reference in each chamber of the twin calorimeter. 2.6 g of the IKWCC were mixed with 2.4 g of the activator inside a disposable glass ampule bottle. The mixing was done using a Vortex mixer (Fisherbrand) operated at 1200 rpm initially for 90 s, waited for 60 s, then mixed again for 90 s before it was loaded into the calorimeter. The reactions were left for 50 h to complete.

Thermoelectric Performance. The electrical behavior of the samples was analyzed through a two-probe AC impedance spectroscopy measurement, performed with the use of a Novocontrol Alpha-A broadband dielectric spectrometer. Data were recorded over a frequency range of 10 mHz to 10 MHz with a voltage amplitude of 1 V. Subsequently, the conductivity was measured under a heat ramp of 1 °C/min to examine the impact of temperature on conductivity.

An evaluation of the Seebeck behavior of the samples was performed by measuring their open-circuit voltage as a function of time. A custom-built experimental setup, depicted in Figure 2, was used to carry out the Seebeck measurements. The prismatic samples, with dimensions of 2 × 2 × 7.5 cm^3 were polished on both sides using sandpapers up to 400 meshes and coated with copper adhesive. The use of silver paste and a thin copper adhesive with a 4 mm spacing between the hot and cold sides to record the thermoelectric voltage of the samples is presented in Figure 2. The samples were subjected to different temperatures using a small ceramic heating plate located on the upper end of the samples. The temperature on each side of the wire connection was measured by a P-type thermocouple connected to a data logger. The voltage difference between the two copper connections was monitored using a KEITHLEY 2100 6 1/2 DIGIT Multimeter and Labview software.

The measurement of thermal conductivity was performed using the modulated differential scanning calorimeter (Q2000 TMDSC-TA) instrument. This methodology involved measuring a thin and thick disk of the same specimen with a diameter
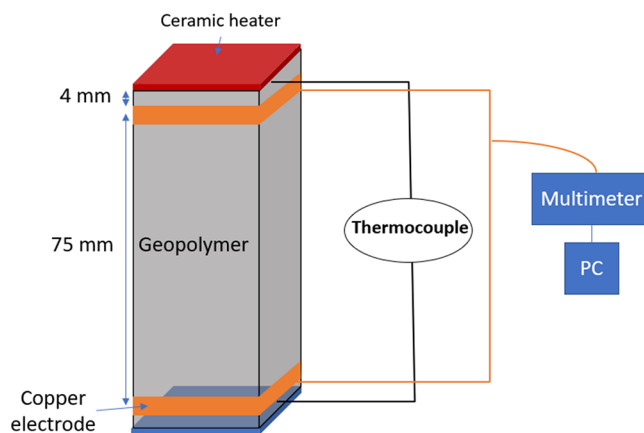

Figure 2. Experimental setup of Seebeck measurement.

of d = 5.2 mm. The thin disk (h < 0.5 mm) was analyzed to determine the specific heat capacity (C_P), as the specimen's thickness was less than the temperature penetration length, resulting in a shorter time for the sample to reach temperature equilibrium. Meanwhile, the thick disk (h = 1.5 mm) was also measured, resulting in the determination of the apparent heat capacity (C). This value was lower than that of the thin disk, due to the nonuniform temperature distribution over the height of the sample. The specific heat capacity (C_P) and the apparent heat capacity (C) were then related to the thermal conductivity through the equation[40]:

$$\lambda = (8LC^2)/(C_P M d^2 P) \tag{1}$$

where λ is the observed thermal conductivity in W/(K m), C is the apparent heat capacity in mJ/K for the thick sample, C_P is the specific heat capacity in J/(g K) for the thin sample, L is the sample height in mm for the thick sample, M is the thick sample mass in mg, d is the thick sample diameter in mm, and P is the modulation period in s.

■ RESULTS AND DISCUSSION

Characterization of Raw and Calcined IKW Clay. The TGA/DTG curves of the IKW clay are illustrated in Figure 3a. The weight loss is almost constant up to 400 °C. In this temperature range, such decrease is related to the loss of adsorbed water on the external surfaces of the raw clay due to dehydration reaction. Major weight loss occurred between the temperature range of 400−700 °C. This reflects the dehydroxylation of the raw clay due to the transformation of the mineral kaolinite in the clay to metakaolinite, also called calcined clay ($2Al_2Si_2O_5(OH)_4 \rightarrow 2Al_2Si_2O_7 + 4H_2O$). The weight loss within this temperature range was about 12.1% which signified the kaolinite content in the clay. Finally, the maximum dehydroxylation temperature of 700 °C was used to calcine the clay.

The oxide composition (wt %) of the calcined clay is given in Table 1. Silica (SiO_2) and Al_2O_3 were the main oxide components of the clay while anatase (TiO_2) and Fe_2O_3 were also present in considerable amounts.

The ratio of SiO_2/Al_2O_3 of IKW is 1:3. The silica-to-alumina ratio for high kaolinite clay is 1:1.[41] This confirms that IKW is a high kaolinite clay as also observed in the TGA curve (Figure 3a). This presents IKW as a good material for geopolymer formation. The detection of K_2O in the clay indicates the presence of Illite.
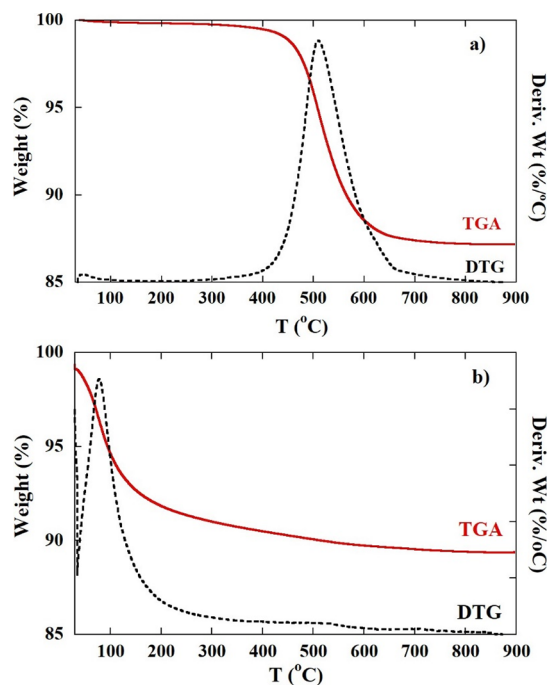
Figure 3. TGA/DTG curves of the three IKW raw clay (a) and IKW-geopolymer (b).
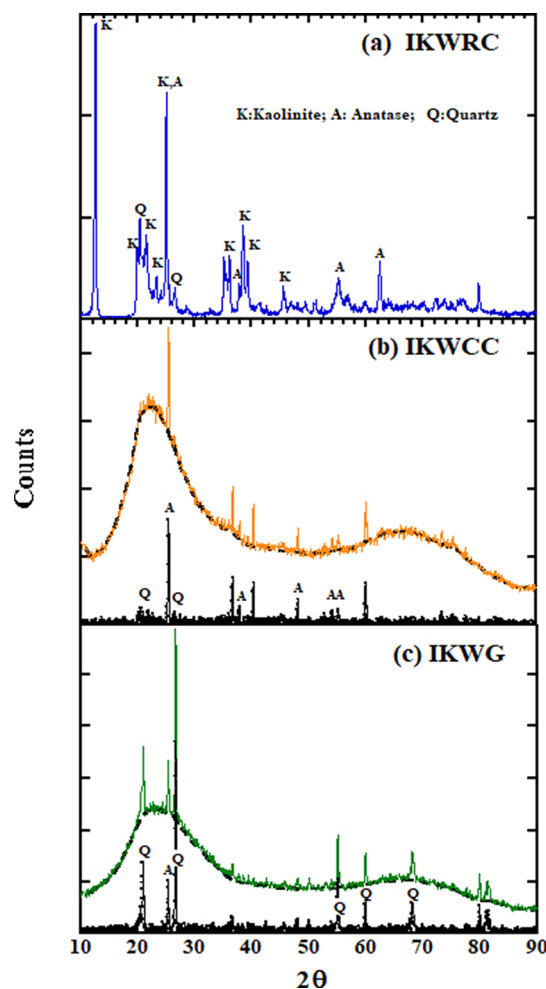

Figure 4. XRD patterns of IKW raw clay IKWRC (a), calcined clay IKWCC (b), and geopolymer IKWG (c). In (b) and (c), the estimated amorphous contribution (dashed lines) has been subtracted, yielding the crystalline contribution (black lines). From comparison with kaolinite, anatase, and quartz patterns, the (at least partial) origin of the main crystalline peaks in (a−c) has been deduced.

The XRD patterns of the IKW raw clay (IKWRC) and IKWCC are shown in Figure 4a,b. In the raw clay, kaolinite was identified as the main chemical phase. In addition, some peaks in this diffractogram would suggest contributions of amounts of quartz and anatase. The presence of anatase confirms the considerable amount of TiO_2 in the clay as observed by XRF. The main effect of calcination is the transformation of the kaolinite in metakaolinite,[39] as demonstrated by the disappearance of the sharp refection peaks corresponding to kaolinite and the emergence of a broad amorphous halo centered at about $2\theta \approx 25°$ (Figure 4b). The estimated amorphous contribution has been subtracted from the experimental results to yield, within the uncertainties, the contribution of the crystalline phases to the pattern. Most of the sharp intense peaks obtained can be attributed to anatase, suggesting that this compound was not affected by temperature during the calcination process. The results show other contributions that could correspond to quartz and other nonidentified phases.

The FTIR spectra showing the main functional groups of the raw and calcined clay are depicted in Figure 5a,b. The absorption bands at 3698 and 3620 cm^{-1} were attributed to the stretching vibrations of OH bonds that are attached to the Al octahedron sheet.[39] Absorption bands associated with stretching Si−O−T (T = Si or Al) vibrations were observed at around wavelengths 1112 and 1005 cm^{-1}. Al−OH bending vibrations due to inner hydroxyl groups were observed in the raw clay at wavelength 908 cm^{-1}. Moreover, a doublet identified at 801 and 753 cm^{-1} has been associated with Si−O stretching vibrations of quartz crystals. The Si−O bending vibration due to the presence of quartz was also observed at

538 cm^{-1}. These results agree with results of XRD analysis (Figure 4) that indicated that IKW also contained quartz. Significant changes were observed in the FTIR spectrum of calcined clay compared with that of the raw clay. The broad bands of the OH groups in the crystalline kaolinite of the raw clay disappeared in the FTIR spectra of calcined clay.

Al−OH bending vibrations at 908 cm^{-1} corresponding to octahedral coordination (AlVI) in the raw clay disappeared and new bands indicating tetrahedral coordination (AlIV) appeared at 811 cm^{-1}. These bands show the ability of this clay to undergo alkaline silicate reactions to form a geopolymer.

Reactivity Study by Isothermal Conduction Calorimetry. The results of normalized heat flow and total heat released from the geopolymerization reactions of the IKW clay measured by isothermal conduction calorimetry are given in Figure 6. As shown, the geopolymerization process involved

Table 1. Oxide Composition of IKW Clay (wt %) Also Present in Considerable Amounts

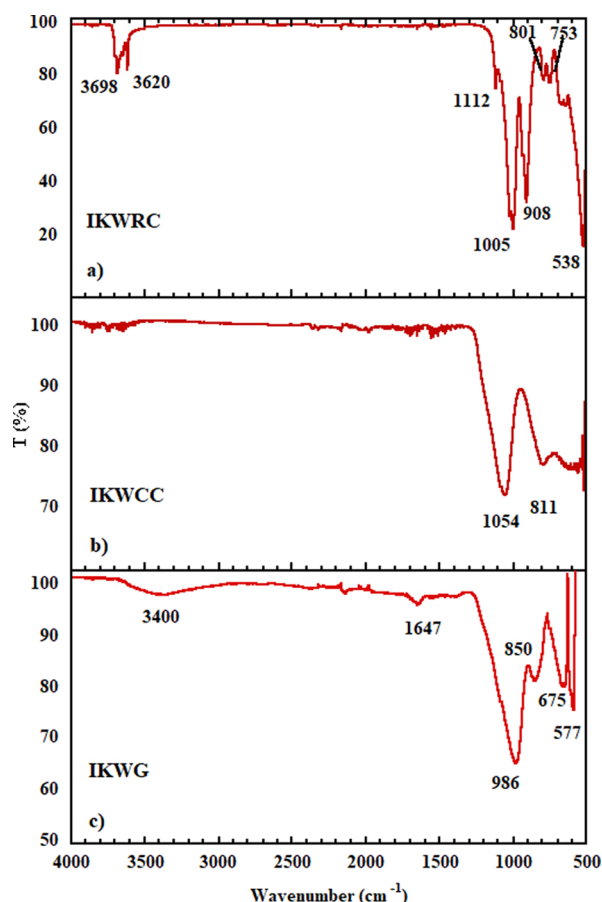| clay	SiO₂	Al₂O₃	Fe₂O₃	MnO	MgO	CaO	K₂O	TiO₂	P₂O₅	SO₃
IKW	53.9	40.2	0.59	0.02	0.12	0.03	0.05	2.08	0.05	0.03

Figure 5. ATR-FTIR spectra of (a) IKW raw clay (IKWRC), (b) calcined clay (IKWCC), and (c) geopolymer (IKWG).

IKWCC and the activator were mixed outside the calorimeter and such a process starts when the activator is mixed with the solid material, the maximum P1 could not be detected from the mix of the clay with the activator (P2). This peak is associated with the reactions producing the first formation of alumina/silica-hydroxy species and their geopolymerization leading to the production of N−A−S−H gel.[42] After 48 h the reactions were almost complete with cumulative heat of 108 J/ g. These observations confirm that IKW formed geopolymer.

Structural Characterization of Geopolymer. The results of the TGA/DTG analysis of the geopolymer are displayed in Figure 3b. Most of the weight loss (9.6 wt %) occurred at temperatures below 180 °C. Over the entire temperature range examined (30−900 °C), a total weight loss of 12.3 wt % was measured. This observation has been reported in previous research to be caused by the evaporation of water from cavities and loosely bound water.[43] The thermal degradation that takes place between 180 and 350 °C (1.4 wt %) is the result of the outgassing of structural water in the sodium aluminosilicate.[44] Finally, the remaining weight loss (1.15 wt %) can be explained by the dehydroxylation of OH silanol or aluminol groups.[45]

The XRD pattern of IKW-geopolymer is illustrated in Figure 4c. It displays a pronounced diffuse peak that confirms IKW-geopolymer predominant amorphous nature resulting from the formation of sodium aluminosilicate (N−A−S−H) gel. In addition, the main sharp peaks in the geopolymer superposed to the amorphous contribution suggest contributions of quartz and anatase. We remember that we could find hints of them also in the diffractogram of the calcined clay (Figure 4b). This is an indication that these minerals did not participate in the geopolymer reaction.

The FTIR spectra of the IKW-geopolymer are shown in Figure 5c. The absorption peaks found at 3400 and 1647 cm^{-1} are due to the presence of both atmospheric and bound water in the geopolymer. These findings are supported by previous research.[39] The intense peak observed at around 986 cm^{-1}, which has replaced the band found in calcined clay at around 1054 cm^{-1}, is associated with the vibration of Si−O in the geopolymer. This shift is due to the substitution of Si−O−Si bonds with Si−O−Al bonds, leading to the formation of N−A−S−H gel in the geopolymer. The peak at around 850 cm^{-1} is attributed to the noncondensed bending vibration of Si−OH.[43] Finally, the peaks found at around 577 and 675 cm^{-1} represent the bending vibration of Si−O−Al.[46]

two stages: dissolution/hydrolysis of the reactive or amorphous contents of the clays (Peak 1, P1) and geopolymer formation (Peak 2, P2) as reported previously.[39] In between the stages is the dormancy stage where the concentration of the dissolved ions grows reaching the threshold for the reactions leading to geopolymerization and condensation of the geopolymer gels. The first peak is a strongly exothermic process and can be considered comparable to the preinduction period of the cement hydration process. After the initial dissolution, the dormant process takes place. Finally, after about 1 h, a broad and intense exothermic peak appeared which reached its maximum after 3 h. Since in this study,
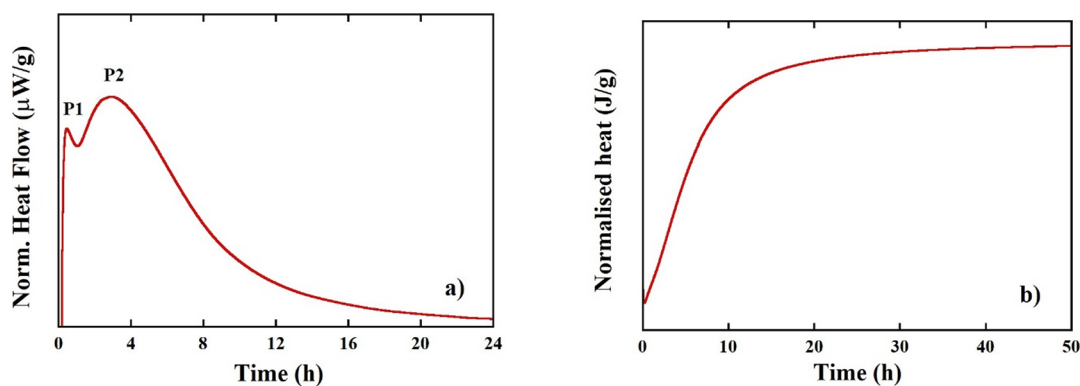

Figure 6. Curves of heat flow (a) and total quantity of heat released (b) of IKW calcined clay.

Thermal and Electrical Characterization of IKW-Geopolymer. The thermal characterization of IKW-geopolymer is shown in Figure 7. In the temperature range
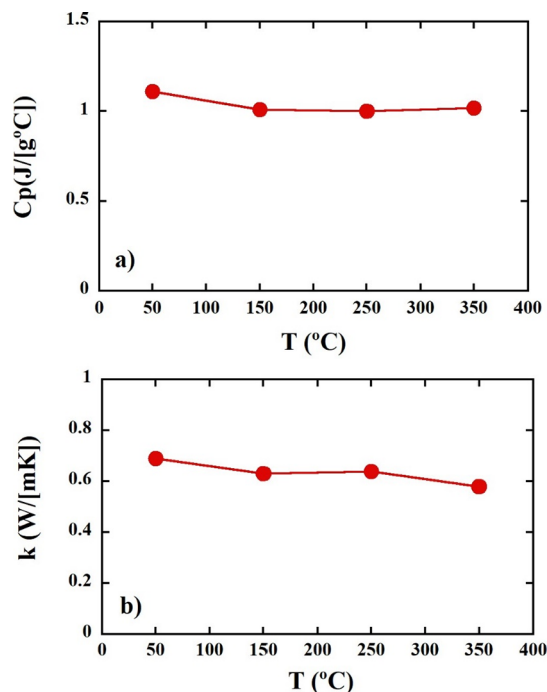

Figure 7. Specific heat capacity (a) and thermal conductivity (b) as a function of temperature of IKW-geopolymer (W/m K) and minimum at $T = 350$ °C ($k = 0.576$ W/m K).

investigated, $50 < T < 350$ °C, the heat capacity shows a stable behavior, with an average C_P of ~0.975 J/°C m. Considering thermal conductivity, a slight decrease is observed over temperature with the maximum value measured at $T = 50$ °C ($k = 0.69$ W/m K) and minimum at $T = 350$ °C ($k = 0.576$ W/m K). Such values are comparable to those reported for other cementitious materials exhibiting thermoelectric behavior. In particular, the results of this study are similar to those obtained for cement with metal oxide nanoparticles.[47]

Understanding the mechanisms underlying the electrical conductivity of cementitious materials is crucial for identifying the optimal temperature range for thermoelectric performance, and for enhancing mix designs to improve the material's figure of merit. For this reason, a deep investigation of the electrically conductive property of the geopolymer was carried out. In Figure 8, the real part of the complex conductive function $\sigma'(f)$ measured by impedance spectroscopy at 300 K is shown. Linear response theory explains that AC spectra of the system are associated with temperature-dependent movements of mobile charges.[48] At high frequencies, the mean square displacement $<r^2(t)>$ exhibits subdiffusive motion and $\sigma'(f)$ shows a frequency-dependent behavior due to ion−ion environment coupling. When the frequency is below the threshold frequency f_0, charge carriers responsible for electrical conductivity change from subdiffusive to diffusive motion, leading to frequency-independent behavior. The decrease of $\sigma'(f)$ observed in the low-frequency range is attributed to electrode polarization.[49] Impedance spectroscopy data were therefore analyzed by means of the Jonsher power law:

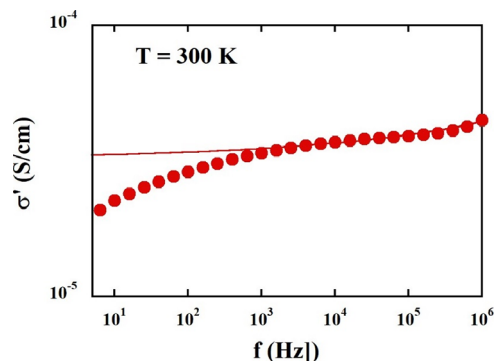$$\sigma(f) = \sigma_{DC}[1 + (f/f_0)^n] + Af \qquad (2)$$

Figure 8. Real part of complex conductive function measured by impedance spectroscopy as a function on frequency at 300 K, with the line representing the fitted model.

where σ_{DC} is the direct current, f_0 is related to the onset of the diffusive motion, n is related to the dimensionality of the charge motion, and A is the nearly constant loss (a contribution coming from frequencies higher than the experimental window).

In Figure 9, the results of the fitting analysis performed are presented. The electrical conductivity starts by increasing and
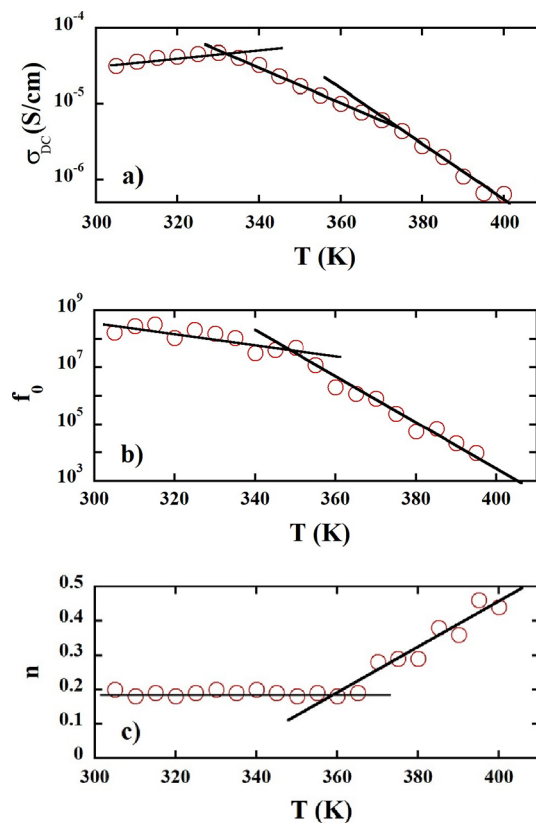

Figure 9. Fitting results of electrical conductivity (a) direct current, (b) onset of the diffusive motion, and (c) dimensionality of the charge motion.

reaches a maximum value of 5.1×10^{-5} S/cm at $T = 330$ K. Subsequently, a decrease is observed as temperature increases, which can be divided into two regimes based on the slope: a slow decrease from 330 to 370 K and a sharp decrease for temperatures above 370 K. The critical temperature, above which a drop in conductivity occurs, is associated with the

evaporation of bulk water from the large pores. This behavior suggests that the ionic contribution is the dominant factor in electrical conductivity. An examination of the temperature dependence of the parameters n and f_0 provides further insight. At low temperatures, n values were found to be around 0.2. However, at temperatures greater than 360 K, a sharp increase in n was observed. A value of n less than 0.5 implies a one-dimensional motion of charge carriers, while a value of n around 0.7 indicates a three-dimensional motion.[50] This suggests a change in the dimensionality of the mechanism responsible for electrical conductivity in IKW-geopolymer as the temperature surpasses $T = 360$ K, going from a 1D displacement (diffusion) toward a 3D (back and forward hopping). A similar trend was noted for f_0, with a similar threshold temperature, in agreement with a change of main contributor to electrical conductivity. Moreover, such a critical temperature is slightly higher than the peak observed on the derivative curve of TGA data associated with the loss of bulk water in the sample. The findings presented in this study suggest the following scenario for the electrical conductivity of IKW-geopolymer network at different temperatures. At low temperatures, the main contributors to electrical conductivity are the ions present in bulk water within the large channels of the geopolymer network. As the temperature increases above the critical $T = 330$ K, bulk water begins to evaporate, leading to a decrease in direct current. However, the motion of the charge carriers remains unchanged suggesting that the presence of bulk water in smaller pores is still the main contributor to electrical conductivity. When the temperature reaches 360−370 K, a transformation occurs, with the charge carriers transitioning from 1D to 3D motion followed by a stronger decrease in conductivity. This change can be attributed to the complete evaporation of bulk water and the subsequent major contribution of electrical conductivity from structural water on the surface of the geopolymer porous network.

Thermoelectric Behavior of IKW-Geopolymer. Figure 10 depicts the Seebeck voltage profile as a function of time.
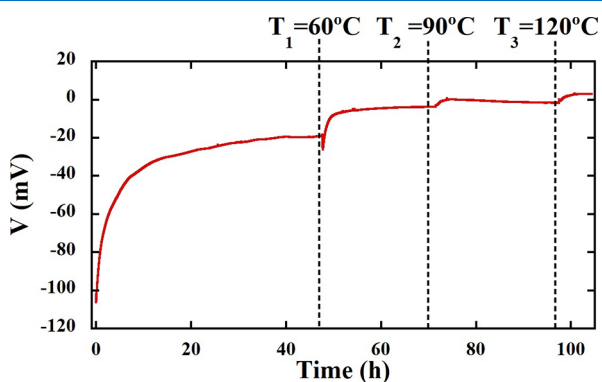
Figure 10. Seebeck voltage profile as a function of time.

Prior to applying any temperature, a high intrinsic voltage of −106 mV was observed, as previously reported in the literature.[28,51,52] To extract information solely on thermoelectric behavior of a material, stabilization of the intrinsic voltage is necessary. After 40 h, a stable value of $V = -19.6$ mV was recorded and a temperature of $T_1 = 60$ °C was applied to the sample through a ceramic heater. Figure 11a illustrates the response of the IKW-geopolymer to the temperature gradient.
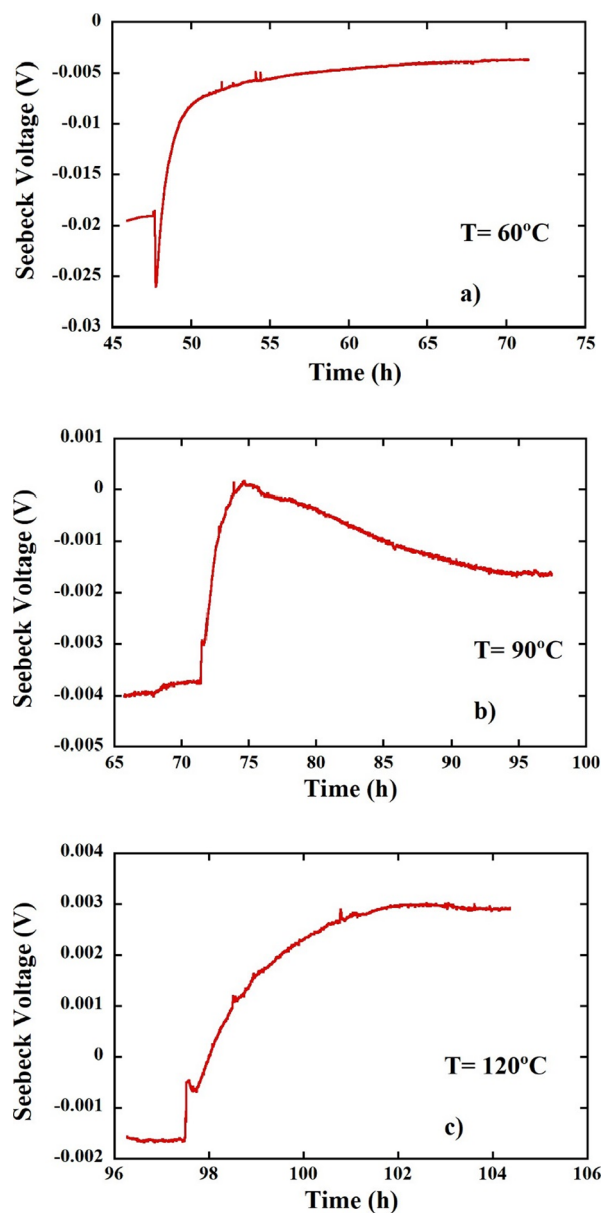
Figure 11. Seebeck voltage measured for different applied temperatures: (a) $T = 60$ °C, (b) 90 °C, and (c) 120 °C.

Initially, a sharp increase in voltage was observed, reaching −26.1 mV within 5 min, followed by a significant decrease. This decrease gradually slowed down after approximately 1 h. Finally, after another 25 h, a new stable voltage value was recorded ($V = -3.9$ mV). The origin of thermoelectric behavior in cementitious materials remains debatable. However, recent studies suggest that ions contribute significantly to thermoelectric behavior.[15,28] In accordance with this scenario, the behavior observed in this work suggests that positive ions (i.e., Na+ from the activator) initially move toward the cold side of the sample, leading to a steep increase in voltage, followed by the response of negative ions (i.e., OH−) to the applied gradient. The prolonged stabilization time reflects the complex mechanism of thermoelectric in cementitious materials, including changes in temperature gradient over time and displacement of ions from their original site, as well as ion accumulation and charge redistribution in the porous network. When a higher temperature of $T_2 = 90$ °C was

applied to the sample, a decrease in voltage was observed, reaching a minimum value of 0.15 mV after approximately 3 h (Figure 11b). This suggests that negative ions are moving toward the cold side of the sample. However, a subsequent increase in voltage was observed, reaching a stable value of Seebeck voltage $V = -1.6$ mV after 25 h from the application of T_2. This indicates a contribution from positive ions or a reduction in negative charges involved in the mechanism. This behavior can be explained by considering that the applied temperature exceeds the temperature at which water outgasses from the large pores, as confirmed by TGA and electrical conductivity measurements. As a result, the hot portion of the sample continuously loses water molecules, resulting in the removal of negative ions. When a temperature of $T_3 = 120$ °C was applied to the sample, the Seebeck voltage increased, and a faster stabilization was reached, taking only 7 h and reaching a final voltage of $V = 2.9$ mV (see Figure 11c). The Seebeck coefficient ($S = \Delta V/\Delta T$) was calculated and is shown in Figure 12a. The Seebeck coefficients are comparable to current state-
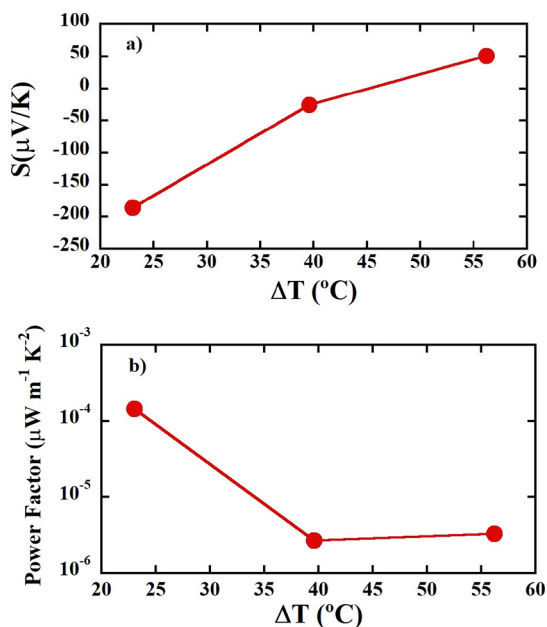

Figure 12. (a) Seebeck coefficient and (b) thermoelectric power factor of IKW-geopolymer.

of-the-art values for cementitious materials and geopolymers (they range from -182 to 42 μV/K). It should be noted, however, that there is no standard method for measuring thermoelectric voltage. As an inherent voltage was observed in this study, a unique experimental design was employed to minimize its contribution, differing from previous approaches in cementitious materials. Moreover, a flip from negative (n-type) to positive (p-type) behavior was observed as the ΔT was increased. This dual nature of IKW-geopolymer, dependent on the ions contributing to the thermoelectric voltage, holds potential for the development of a solid-state ionic thermoelectric capacitor (ITEC).[53] In Figure 12b, the calculated thermoelectric power factor of the IKW-geopolymer is presented. A notable decrease is observed at higher temperature differences, primarily attributed to a significant reduction in electrical conductivity

CONCLUSIONS

This study provides valuable insights into the thermoelectric behavior of the geopolymer, which is made from kaolinite clay. An understanding of the mechanisms influencing the performance of the geopolymer as a thermoelectric and its potential for energy conversion and storage applications was achieved in the study.

Regarding the thermal properties, the thermal conductivity decreases slightly as the temperature increases, with the highest value of 0.69 W/m K recorded at 50 °C and the lowest value of 0.576 W/m K recorded at 350 °C, comparable with the state-of-the-art thermoelectric materials.

The electrical conductivity measurements revealed that, at low temperatures, the primary contributors to electrical conductivity were the ions present in bulk water within the large channels of the geopolymer network. However, as temperature increases above a critical value, bulk water began to evaporate and the charge carriers transition from 1D to 3D motion, resulting in a decrease in conductivity. The electrical conductivity was found to be in the range of 5×10^{-5}–6×10^{-7} S/cm.

The Seebeck coefficient measurements suggest that ions may be the source of thermoelectric in cementitious materials, with positive ions initially moving toward the cold side of the sample and negative ions subsequently responding to the applied temperature gradient. The Seebeck coefficients measured ranged from -182 to 42 μV/K, which are comparable to values obtained in current state-of-the-art studies. The origin and temperature profile of the electrical conductivity in the thermoelectric geopolymer suggests that it can be effectively used in low-temperature applications such as the recovery of low-grade waste heat.

Notably, this study observed a unique n-type to p-type transition, depending on the operating temperature, opening new avenues for thermoelectric capacitors.

Conclusively, the thermoelectric behavior of the IKW-geopolymer holds great potential for energy conversion and storage applications. Its unique properties can be exploited for the development of a sustainable structural element as a state solid thermoelectric generator.

AUTHOR INFORMATION

Corresponding Authors

Guido Goracci — *CSIC-UPV/EHU, Centro de Física de Materiales, 20018 San Sebastián, Spain;* orcid.org/0000-0003-2439-3833; Email: guido.goracci@ehu.eus

Mary B. Ogundiran — *CSIC-UPV/EHU, Centro de Física de Materiales, 20018 San Sebastián, Spain; Analytical/Environmental Unit, Department of Chemistry, Faculty of Science, University of Ibadan, Ibadan 200132, Nigeria;* Email: mbogundiran@gmail.com

Authors

Mohamad Barzegar — *CSIC-UPV/EHU, Centro de Física de Materiales, 20018 San Sebastián, Spain*

Amaia Iturrospe — *Materials Physics Center, 20018 San Sebastián, Spain*

Arantxa Arbe — *CSIC-UPV/EHU, Centro de Física de Materiales, 20018 San Sebastián, Spain*

Jorge S. Dolado — *CSIC-UPV/EHU, Centro de Física de Materiales, 20018 San Sebastián, Spain; Donostia International Physics Center, 20018 San Sebastián, Spain;* orcid.org/0000-0003-3686-1438

■ REFERENCES

(1) Ovik, R.; Long, B. D.; Barma, M. C.; Riaz, M.; Sabri, M. F. M.; Said, S. M.; Saidur, R. A Review on Nanostructures of High-Temperature Thermoelectric Materials for Waste Heat Recovery. *Renew Sustain. Energy Rev.* **2016**, *64*, 635−659, DOI: 10.1016/j.rser.2016.06.035.

(2) Patil, D. S.; Arakerimath, R. R.; Walke, P. V. Thermoelectric Materials and Heat Exchangers for Power Generation − A Review. *Renew. Sustain. Energy Rev.* **2018**, *95*, 1−22.

(3) Brückner, S.; Liu, S.; Miró, L.; Radspieler, M.; Cabeza, L. F.; Lävemann, E. Industrial Waste Heat Recovery Technologies: An Economic Analysis of Heat Transformation Technologies. *Appl. Energy* **2015**, *151*, 157−167.

(4) Ebrahimi, K.; Jones, G. F.; Fleischer, A. S. A Review of Data Center Cooling Technology, Operating Conditions and the Corresponding Low-Grade Waste Heat Recovery Opportunities. *Renew. Sustain. Energy Rev.* **2014**, *31*, 622−638.

(5) Massetti, M.; Jiao, F.; Ferguson, A. J.; Zhao, D.; Wijeratne, K.; Würger, A.; Blackburn, J. L.; Crispin, X.; Fabiano, S. Unconventional Thermoelectric Materials for Energy Harvesting and Sensing Applications. *Chem. Rev.* **2021**, *121* (20), 12465−12547.

(6) Hasan, M. N.; Wahid, H.; Nayan, N.; Mohamed ali, M. S. Inorganic Thermoelectric Materials: A Review. *Int. J. Energy Res.* **2020**, *44* (8), 6170−6222.

(7) Soleimani, Z.; Zoras, S.; Ceranic, B.; Shahzad, S.; Cui, Y. A Review on Recent Developments of Thermoelectric Materials for Room-Temperature Applications. *Sustain. Energy Technol. Assess.* **2020**, *37*, 100604.

(8) Witting, I. T.; Chasapis, T. C.; Ricci, F.; Peters, M.; Heinz, N. A.; Hautier, G.; Snyder, G. J. The Thermoelectric Properties of Bismuth Telluride. *Adv. Electron. Mater.* **2019**, *5* (6), 1−20.

(9) Mamur, H.; Bhuiyan, M. R. A.; Korkmaz, F.; Nil, M. A Review on Bismuth Telluride (Bi2Te3) Nanostructure for Thermoelectric Applications. *Renew. Sustain. Energy Rev.* **2018**, *82*, 4159−4169.

(10) Rogl, G.; Rogl, P. Skutterudites, a Most Promising Group of Thermoelectric Materials. *Curr. Opin. Green Sustain. Chem.* **2017**, *4*, 50−57.

(11) Tong, X.; Liu, Z.; Zhu, J.; Yang, T.; Wang, Y.; Xia, A. Research Progress of P-Type Fe-Based Skutterudite Thermoelectric Materials. *Front. Mater. Sci.* **2021**, *15* (3), 317−333.

(12) Basu, R.; Singh, A. High Temperature Si−Ge Alloy towards Thermoelectric Applications: A Comprehensive Review. *Mater. Today Phys.* **2021**, *21*, 100468.

(13) Singh, V. P.; Kumar, M.; Srivastava, R. S.; Vaish, R. Thermoelectric Energy Harvesting Using Cement-Based Composites: A Review. *Mater. Today Energy* **2021**, *21*, No. 100714.

(14) Ghosh, S.; Harish, S.; Rocky, K. A.; Ohtaki, M.; Saha, B. B. Graphene Enhanced Thermoelectric Properties of Cement Based Composites for Building Energy Harvesting. *Energy Build.* **2019**, *202*, 109419.

(15) Wei, Y.; Cui, Y.; Wang, Y. Ionic Thermoelectric Effect of Pure Cement Paste and Its Temperature Sensing Performance. *Constr. Build. Mater.* **2023**, *364*, No. 129898, DOI: 10.1016/j.conbuildmat.2022.129898.

(16) Wan, Y.; Tan, S.; Li, L.; Zhou, H.; Zhao, L.; Li, H.; Han, Z. Fabrication and Thermoelectric Property of the Nano Fe2O3/Carbon Fiber/Cement-Based Composites for Potential Energy Harvesting Application. *Constr. Build. Mater.* **2023**, *365*, 130021.

(17) Ghosh, S.; Harish, S.; Ohtaki, M.; Saha, B. B. Thermoelectric Figure of Merit Enhancement in Cement Composites with Graphene and Transition Metal Oxides. *Mater. Today Energy* **2020**, *18*, No. 100492.

(18) Vareli, I.; Tzounis, L.; Tsirka, K.; Kavvadias, I. E.; Tsongas, K.; Liebscher, M.; Elenas, A.; Gergidis, L. N.; Barkoula, N. M.; Paipetis, A. S. High-Performance Cement/SWCNT Thermoelectric Nanocomposites and a Structural Thermoelectric Generator Device towards Large-Scale Thermal Energy Harvesting. *J. Mater. Chem. C* **2021**, *9* (40), 14421−14438.

(19) Wei, J.; Zhao, L.; Zhang, Q.; Nie, Z.; Hao, L. Enhanced Thermoelectric Properties of Cement-Based Composites with Expanded Graphite for Climate Adaptation and Large-Scale Energy Harvesting. *Energy Build.* **2018**, *159*, 66−74.

(20) Liu, X.; Jani, R.; Orisakwe, E.; Johnston, C.; Chudzinski, P.; Qu, M.; Norton, B.; Holmes, N.; Kohanoff, J.; Stella, L.; et al. State of the Art in Composition, Fabrication, Characterization, and Modeling Methods of Cement-Based Thermoelectric Materials for Low-Temperature Applications. *Renew. Sustain. Energy Rev.* **2021**, *137*, No. 110361.

(21) Cui, Y.; Wei, Y. Mixed "Ionic-Electronic" Thermoelectric Effect of Reduced Graphene Oxide Reinforced Cement-Based Composites. *Cem. Concr. Compos.* **2022**, *128*, 104442.

(22) Ji, T.; Zhang, S.; He, Y.; Zhang, X.; Zhang, X.; Li, W. Enhanced Thermoelectric Property of Cement-Based Materials with the Synthesized MnO2/Carbon Fiber Composite. *J. Build. Eng.* **2021**, *43*, 103190.

(23) Ghahari, S. A.; Ghafari, E.; Lu, N. Effect of ZnO Nanoparticles on Thermoelectric Properties of Cement Composite for Waste Heat Harvesting. *Constr. Build. Mater.* **2017**, *146*, 755−763.

(24) Jani, R.; Holmes, N.; West, R.; Gaughan, K.; Liu, X.; Qu, M.; Orisakwe, E.; Stella, L.; Kohanoff, J.; Yin, H.; et al. Characterization and Performance Enhancement of Cement-Based Thermoelectric Materials. *Polymers (Basel).* **2022**, *14* (12), 2311.

(25) Cai, J.; Li, X. Thermoelectric Properties of Geopolymers with the Addition of Nano-Silicon Carbide (SiC) Powder. *Ceram. Int.* **2021**, *47*, 19752−19759.

(26) Cai, J.; Tan, J.; Li, X. Thermoelectric Behaviors of Fly Ash and Metakaolin Based Geopolymer. *Constr. Build. Mater.* **2020**, *237*, No. 117757, DOI: 10.1016/j.conbuildmat.2019.117757.

(27) Li, J.; Tay, B. W. Y.; Lei, J.; Yang, E. H. Experimental Investigation of Seebeck Effect in Metakaolin-Based Geopolymer. *Constr. Build. Mater.* **2021**, *272*, No. 121615.

(28) Barzegar, M.; Goracci, G.; Martauz, P.; Dolado, J. S. Sustainable Geopolymer Concrete for Thermoelectric Energy Harvesting. *Constr. Build. Mater.* **2024**, *411*, No. 134398.

(29) Davidovits, J. Geopolymers - Inorganic Polymeric New Materials. *J. Therm. Anal.* **1991**, *37* (8), 1633−1656.

(30) Cui, X. M.; Liu, L. P.; He, Y.; Chen, J. Y.; Zhou, J. A Novel Aluminosilicate Geopolymer Material with Low Dielectric Loss. *Mater. Chem. Phys.* **2011**, *130* (1−2), 1−4.

(31) Mehta, A.; Siddique, R. An Overview of Geopolymers Derived from Industrial By-Products. *Constr. Build. Mater.* **2016**, *127*, 183−198, DOI: 10.1016/j.conbuildmat.2016.09.136.

(32) Palomo, A.; Grutzeck, M. W.; Blanco, M. T. Alkali-Activated Fly Ashes A Cement for the Future. *Cem. Concr. Res.* **1999**, *29*, 1323−1329, DOI: 10.1016/S0008-8846(98)00243-9.

(33) Shi, C.; Jiménez, A. F.; Palomo, A. New Cements for the 21st Century: The Pursuit of an Alternative to Portland Cement. *Cem. Concr. Res.* **2011**, *41* (7), 750−763.

(34) Provis, J. L.; Palomo, A.; Shi, C. Advances in Understanding Alkali-Activated Materials. *Cem. Concr. Res.* **2015**, *78*, 110−125.

(35) Singh, N. B.; Middendorf, B. Geopolymers as an Alternative to Portland Cement: An Overview. *Constr. Build. Mater.* **2020**, *237*, No. 117455, DOI: 10.1016/j.conbuildmat.2019.117455.

(36) Li, N.; Shi, C.; Zhang, Z.; Wang, H.; Liu, Y. A Review on Mixture Design Methods for Geopolymer Concrete. *Compos. Part B Eng.* **2019**, *178*, No. 107490, DOI: 10.1016/j.composi-tesb.2019.107490.

(37) Mclellan, B. C.; Williams, R. P.; Lay, J.; Van riessen, A.; Corder, G. D. Costs and Carbon Emissions for Geopolymer Pastes in Comparison to Ordinary Portland Cement. *J. Clean. Prod.* **2011**, *19* (9−10), 1080−1090.

(38) Yu, X.; Chen, L.; Komarneni, S.; Hui, C. Fly Ash-Based Geopolymer: Clean Production, Properties and Applications. *J. Clean. Prod.* **2016**, *125*, 253−267.

(39) Ogundiran, M. B.; Kumar, S. Applied Clay Science Synthesis and Characterisation of Geopolymer from Nigerian Clay. *Appl. Clay Sci.* **2015**, *108*, 173−181.

(40) Foreman, J. A.; Marcus, S. M.; Blaine, R. L. Thermal Conductivity of Polymers, Glasses & Ceramics by Modulated DSC. *Annu. Technol. Conf. - ANTEC, Conf. Proc.* **1994**, No. No. pt 2, 2156−2158.

(41) Adeniyi, F. I.; Ogundiran, M. B.; Hemalatha, T.; Hanumantrai, B. B. Characterization of Raw and Thermally Treated Nigerian Kaolinite-Containing Clays Using Instrumental Techniques. *SN Appl. Sci.* **2020**, *2* (5), 1−14.

(42) Yao, X.; Zhang, Z.; Zhu, H.; Chen, Y. Geopolymerization Process of Alkali − Metakaolinite Characterized by Isothermal Calorimetry. *Thermochim. Acta* **2009**, *493*, 49−54, DOI: 10.1016/j.tca.2009.04.002.

(43) Tchakouté, H. K.; Rüscher, C. H.; Kong, S.; Kamseu, E.; Leonelli, C. Comparison of Metakaolin-Based Geopolymer Cements from Commercial Sodium Waterglass and Sodium Waterglass from Rice Husk Ash. *J. Sol-Gel Sci. Technol.* **2016**, *78*, 492−506, DOI: 10.1007/s10971-016-3983-6.

(44) Rosas-casarez, C. A.; Arredondo-rea, S. P.; Gómez-Soberón, J. M.; Almaral-Sánchez, J. L.; Corral-Higuera, R.; Chinchillas-Chinchillas, M. J.; Acuña-Aguero, O. H. Experimental Study of XRD, FTIR and TGA Techniques in Geopolymeric Materials. *Int. J. Hous. Sci. Appl.* **2014**, *4* (4), 212−227.

(45) Duxson, P.; Lukey, G. C.; Van Deventer, J. S. J. Physical Evolution of Na-Geopolymer Derived from Metakaolin up to 1000° C. *J. Mater. Sci.* **2007**, *42*, 3044−3054, DOI: 10.1007/s10853-006-0535-4.

(46) Tchakouté, H. K.; Rüscher, C. H.; Kong, S.; Kamseu, E.; Leonelli, C. Thermal Behavior of Metakaolin-Based Geopolymer Cements Using Sodium Waterglass from Rice Husk Ash and Waste Glass as Alternative Activators. *Waste Biomass Valor.* **2017**, *8*, 573−584, DOI: 10.1007/s12649-016-9653-7.

(47) Ghahari, S.; Ghafari, E.; Lu, N. Effect of ZnO Nanoparticles on Thermoelectric Properties of Cement Composite for Waste Heat Harvesting. *Constr. Build. Mater.* **2017**, *146*, 755−763.

(48)), 85901−1-85901−85902. doi: Roling, B.; Martiny, C.; Murugavel, S. Ionic Conduction in Glass: New Information on the Interrelation between the "Jonscher Behavior" and the "Nearly Constant-Loss Behavior" from Broadband Conductivity Spectra. *Phys. Rev. Lett.* **2001**, *87*, 8.

(49) Sidebottom, D. L.; Roling, B.; Funke, K. Ionic Conduction in Solids: Comparing Conductivity and Modulus Representations with Regard to Scaling Properties. *Phys. Rev. B - Condens. Matter Mater. Phys.* **2000**, *63* (2), 1−7.

(50) Nowick, A. S.; Vaysleyb, A. V.; Liu, W. Identification of Distinctive Regimes of Behaviour in the Ac Electrical Response of Glasses. *Solid State Ionics* **1998**, *105* (1−4), 121−128.

(51) Li, J.; Wee, B.; Tay, Y.; Lei, J.; Yang, E.-H. Experimental Investigation of Seebeck Effect in Metakaolin-Based Geopolymer. *Constr. Build. Mater.* **2021**, *272*, No. 121615, DOI: 10.1016/j.conbuildmat.2020.121615.

(52) Huang, C. Y.; Chung, D. D. L. Controlling and Increasing the Inherent Voltage in Cement Paste. *Adv. Cem. Res.* **2009**, *21* (1), 31−37.

(53) Cheng, H.; Le, Q.; Liu, Z.; Qian, Q.; Zhao, Y.; Ouyang, J. Ionic Thermoelectrics: Principles, Materials and Applications. *J. Mater. Chem. C* **2022**, *10* (2), 433−450.